한국광물학회지 제 16 권 제 1 호 (2003)
J. Miner. Soc. Korea, 16, 107-123 (2003)

Investigation of Corrosion Minerals from the Remediation for TCE-Contaminated Groundwater

TCE로 오염된 지하수 정화시 부식 광물에 대한 연구

Ji-Won Moon (문지원)[1] · Hi-Soo Moon (문희수)[2]* · Yungoo Song (송윤구)[2] · Jin Kyoo Kang (강진규)[2] · Yul Roh (노 열)[1]

[1] Environmental Sciences Division, Oak Ridge National Laboratory, Oak Ridge, TN 37831-6038, USA
(미국 오크릿지 국립연구소, 환경과학실)
[2] Department of Earth System Sciences, Yonsei University, Shinchon-dong 134, Seodaemun-ku, Seoul 120-749, Korea, E-mail: jwmoon@yonsim.yonsei.ac.kr
(연세대학교 지구시스템과학과)

ABSTRACT : The objective of this study was to investigate mineral precipitates, which derived from the zero valent iron (ZVI) corrosion during TCE dechlorination and to find the controlling factors in mineral precipitates. A series of column experiemnts were conducted to evaluate the location of ZVI and the effects of electrode arrangements in electro-enhanced permeable reactive barrier (E2PRB) systems. Based on mineralogical study, ZVI samples near the influent port had more lepidocrocite, ferrihydrite or Fe (oxy)hydroxide, and (phospho)siderite while backward samples had more akaganeite, magnetite/maghemite, and intermediate green rust (GR) I and GR II. A suite of mineral distribution was preferabley related to the dissolved oxygen and the increased pH. Controlling factors of mineral precipitates in an E2PRB system were found to be (1) pH, (2) dissolved oxygen, (3) the types of Fe intermediates, and (4) anionic species to form complex strongly.

Key words : zero valent iron, corrosion, mineral precipitate, electro-enhanced permeable reactive barrier

요약 : 본 연구는 0가 철 (ZVI)의 설치위치와 전극의 배열에 따른 다양한 조합의 전기적 투수성 반응벽을 대상으로 트리클로로에틸렌의 탈염소화 반응에 의한 정화시 ZVI의 부식에 기인하는 광물상 침전물에 대해 알아보고, 이에 대한 조절 요소를 알아보고자 한다. 광물학적 연구 결과, 지하수 유입부의 ZVI 시료는 상대적으로 많은 레피도크로사이트, 훼리하이드라이트 혹은 철 수산화물과 (phospho)siderite가 산출되는 반면, 용출부의 ZVI 시료는 아카가나이트, 자철석/마그헤마이트, 그리고 중간 산물인 green rust (GR) I 과 GR II가 산출되었다. 이러한 광물 조합의 변화는 용존 산소 및 pH의 상승에 주로 기인한 것으로 나타났다. 또한 전기적 투수성 반응벽 내에 산출되는 광물상 침전물들의 조절 요소들은 (1) pH, (2) 용존산소, (3) 철의 부식시 중간 산물, (4) 음이온 종류 등으로 밝혀졌다.

주요어 : 0가철, 부식, 광물상 침전물, 전기적 투수성 반응벽

*교신저자: hsmoon@yonsei.ac.kr

Introduction

Out of most commonly identified contaminants at hazardous waste sites in the US, 10 are chlorinated organic compounds (COCs), commonly originating as cleaning and degreasing solvents. The use of zero valent iron (ZVI) for in-situ degradation of dissolved COCs is rapidly gaining acceptance as a cost-effective technology for groundwater remediation.

The ZVI media are inexpensive and the most widely used materials that have shown encouraging results in removing contaminants from groundwater (Matheson and Tratnyek, 1994). However, the permeable reactive barrier (PRB) system entrance is plugged due principally to mineral precipitation promoted by dissolved oxygen (DO) in the groundwater inflow (Mackenzie *et al.*, 1999). To control precipitation and hence porosity losses, it is important to investigate precipitated minerals and to understand some factors that affect mineral precipitation under given hydrochemical conditions. Factors that possibly affect the type and extent of precipitation include; pH, carbonate level, iron corrosion rate, and residence time in the system. Major phases in the reactive ZVI barrier installed at several field sites generally include iron oxides, carbonates, iron sulfides, and elemental sulfur depending on the degree of iron oxidation, groundwater chemistry, iron corrosion rate, microbial activity, and residence time in the system. The removal of trichloroethylene (TCE) occurred via reductive dechlorination in the presence of ZVI. In turn, the precipitates crystallize into minerals with several anions.

There are various possible reasons for the different dechlorination efficiency since the reaction rates are sensitive to redox-related parameters including pH, DO, dissolved organics, and anionic species in the groundwater. Anions promote corrosion of ZVI by disrupting the protective oxide layers (Gui and Devine, 1994), thus facilitating continued anodic dissolution of the iron and hydrogen generation (Phelps *et al.*, 1991; Reardon, 1995).

The direct current (DC) applied on the ZVI-based PRB controls the oxidation rate of the iron as electrons transverse an external circuit to a Fe^0 cathode, where they engage in reductive TCE degradation (Roh *et al.*, 2000c; Moon *et al.*, 2001). When, remediating a certain TCE-contaminated site, hydrogeochemical conditions such as kinds and levels of contaminants as well as groundwater chemistry are usually fixed, while engineering factors such as ZVI installation and electrode arrangements must be set for maximum TCE removal in field electro-enhanced permeable reactive barrier (E2PRB) system. The objective of this study was focused on the mineralogical characterization of corrosive precipitates of ZVI media using one or two ZVI zones in the column experiments and controlling factors of ZVI corrosion. Detailed mineralogical characterization is, therefore, imperative to predict the long-term performance of the ZVI-based passive reactive wall.

Materials and Methods

TCE-contaminated Water, Fe^0 Filing Materials, and Column Set-up

Trichloroethylene (99.5%, Sigma-Aldrich)-contaminated groundwater (Table 1) was used for this experiment. During the continuous column experiments, the TCE-contaminated simulation water was kept in a 10 liter-collapsible Tedlar sample bag (SKC Inc., PA) with no headspace and was pumped to the column using a peristaltic pump (Diqi-Staltic, Masterflex, Vernon Hills, IL) at 1 mL/min flow rate. Actual flow rates determined by measuring the discharge were varied from 0.828 to 1.10 mL/min. The consistent TCE concentration levels were kept by stirring the water in Tedlar bags using magnetic stirrer during the experiment.

The ZVI filings are stock Fe^0 filing purchased from Peerless Metal Powders and Abrasives (Detroit, MI). The peerless Fe^0 filings had following characteristics: (1) mesh size between 8 and 50 (i.e., 2.38 to 0.30 mm); (2) 86% Fe^0,

Table 1. Physical characteristics and chemical composition of filing materials and simulated waters

Filing materials		Simulated waters		
			Min	Max
Peerless Fe^0		pH	5.51	6.91
Fe	Fe^0, $Fe^{2+}Fe^{3+}{}_2O_4$	Eh (mV)	612.1	957.9
C (%)	<4	EC (μS/cm)	91.3	196.2
Pb (mg/kg)	58.46	DO (mg/L)	3.62	5.60
Ni (mg/kg)	256.8	Temperature (°C)	18.8	26.9
Co (mg/kg)	946.5	HCO_3^- (mg/L)	7.52	14.98
Mn (mg/kg)	5105	Cl^- (mg/L)	6.20	8.62
Mg (mg/kg)	41.48	NO_3^- (mg/L)	12.02	12.70
Cu (mg/kg)	3823	HPO_4^{2-} (mg/L)	8.94	9.49
Ca (mg/kg)	803.4	SO_4^{2-} (mg/L)	8.99	9.73
Al (mg/kg)	61.1	Na (mg/L)	14.79	20.82
Na (mg/kg)	298	Fe^{2+} (mg/L)	< 0.01	< 0.01
SSA* (m^2/g)	1.213	Total Fe (mg/L)	< 0.01	< 0.01
CEC (meq/mol)	0.56	MES**	597.4	2485
Porosity (%)	65.0	TCE (μg/L)		
Quartz sand				
Porosity (%)	45.0			

*SSA: specific surface area. **MES: [2-(N-morpholino)ethenesufonic acid.

3~4% carbon, <3% silicon and other trace metals; and (3) mostly Fe^0 with tracer amount of magnetite. Iron and other trace metals were measured by inductively coupled plasma-atomic emission spectroscopy (ICP-AES, Jobin Yvon 138 Ultrace) at Seoul Branch of Korea Basic Science Institute (Table 1).

Glass columns (Ace Glass, Vineland, NJ) used for the experiment were 35 cm long with 1.5 cm inner diameter, and had 2 thread ports for electrodes installation at 8 and 27 cm from the inlet. The used electrode material was iridium-coated titanium oxide (3 mm outer-diameter). Both ends were tightly sealed using Teflon thread end fittings and polyethylene filter disc with O-rings. Twelve column set-ups were used to treat TCE-contaminated groundwater with different combination of ZVI installation and electrode arrangement (Fig. 1). In this paper, each type of column set-up was described in italic to reduce confusion such as *A*, *B*, *C*, *D*, *a*, *b*, and *c*. Single E2PRB is defined as a set-up using one ZVI portion such as *Ba~Cc*. On the contrary, double E2PRB is done as a set-up using two ZVI portions such as *Da~Dc*.

A type (*Aa*, *Ab*, *Ac*) columns were controls, tested only the effect of external DC and its electrode arrangement without ZVI. *B* type (*Ba*, *Bb*, *Bc*) and *C* type (*Ca*, *Cb*, *Cc*) simulated conditions that ZVI was installed either at hydraulic up or down gradient. *D* type (double PRB) employed ZVI installation at both up and down gradient sides to test any synergistic effects using two ZVI zones rather than one (*B* and *C* type). Each *a* type is a control without DC. For *b* and *c* type, cathode or anode was connected to an iridium-coated titanium oxide electrode in contact with carbon pad (5 mm thickness, 90±5 mg) at hydraulic up gradient. The remaining column space was packed with quartz sand (15~20 mesh, Junsei Chemical, Japan).

Sampling and Analysis

Dissolved oxygen (DO), pH, Eh, and electric conductivity (EC) were measured in a closed glass micro-cell in line. The pH, Eh, and EC measurements were conducted using an MMS Phuture pH/conductivity meter equipped with

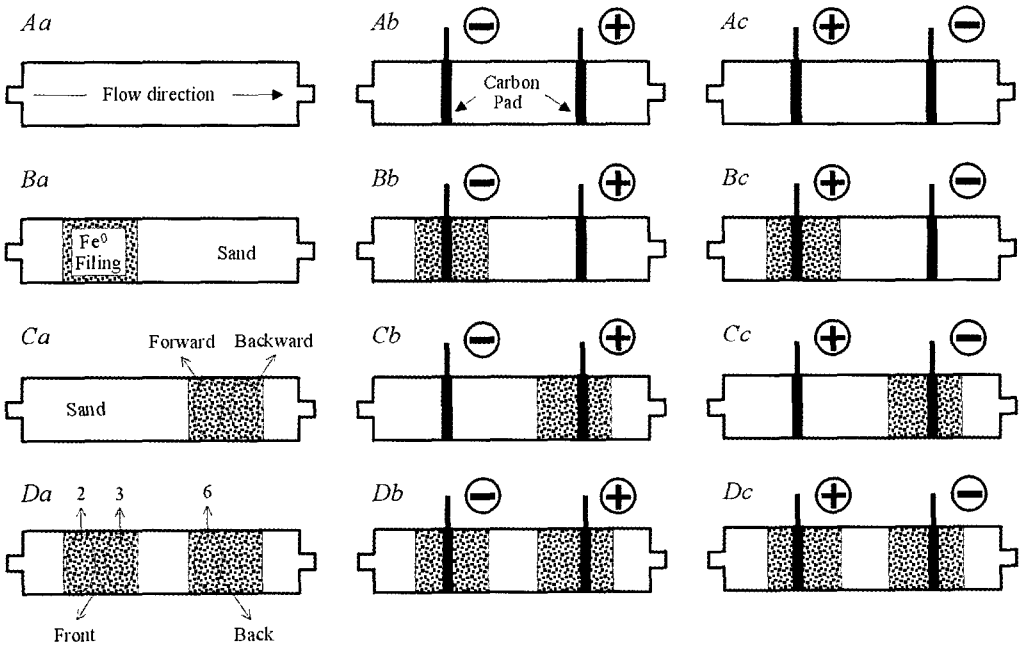

Fig. 1. Schematic diagrams showing experimental setup used for ZVI corrosion.

Pentrode probe (Thermo Orion, Boston, MA). Dissolved oxygen was measured using a combination of Orion DO probe (83005A model) and 830A DO meter (Orion, Berverly, MA). Aqueous samples were collected directly from the sampling port (T-shaped plug valve, Hamilton, Reno, NV) using 20 mL glass syringe adapted with retrofit syringe valve (Alltech, Deerfield, IL) to prevent volatilization of VOCs and oxidation of dissolved iron in the treated water. The C_0 samples were directly collected from the influent using a needle adapted to 20 mL syringe to penetrate Norprene tube. Samples were split into several bottles for measurements of TCE, Fe^{2+}, total Fe, and matrix electrolyte concentrations.

The concentration levels of TCE and by-products were analyzed by Method 5035 purge-and-trap system (SRI, Torrance, CA) and gas chromatography (GC, SRI 8610B, Torrance, CA) equipped with a flame ionization detector (FID). Analyses for the concentration levels of dissolved ferrous iron (Fe^{2+}) and total iron were done by a UV spectrophotometer (UV-1601PC, Shimadzu, Japan), and for the anionic species by high performance liquid chromatography (HPLC, DX-80 Ion Analyzer, Dionex) and 796 Titroprocessor model (Metrohm, Switzerland). Detailed analytical methods were the same as the procedures adopted in Moon *et al* (2002).

Mineralogical Characterization of Precipitates

After the completion of the flow-through experiments, the columns were disassembled. ZVI portion was divided into two parts based on the center of length when ZVI filing was filled in the column (Fig. 1). The filing ZVI materials including corroded samples were immediately rinsed and immersed in acetone for next mineralogical and morphological study. Corroded by-products were separated by sonication (about 1 min). To obtain X-ray diffraction patterns, solid phases immersed in acetone were mounted using transfer pipette, then repeatedly measured when the acetone almost evaporated. A X-ray diffractometer (XRD, MXP-3 system, Mac Science Co., Japan) with Ni-filtered Cu-Kα radiation, 40 kV and 30 mA, divergent and scattering slits of 1 mm, a receiving slit of 0.15 mm and a

0.02°2θ were used. Counting time of 2 sec for each step was set.

A subportion of wet Fe^0 filings was prepared for mineralogical analysis by rapidly drying using an acetone rinse to minimize oxidation, then examined by scanning electron microscopy (SEM) with energy-dispersive X-ray (EDX) analyses (JSM 5600, JEOL, Japan) for surface morphology and the chemical composition of the minerals semi-quantitatively.

Infrared spectra of corroded phases separated by sonification were obtained with a Fourier Tansformed Infrared Spectroscopy (FTIR, IFS 120HR/FRA106, Bruker, Germany) at Daegu Branch of Korea Basic Science Institute with a spectral range from 4,000 to 400 cm^{-1}. The pressed-pellet technique was used to prepare samples for infrared examination by mixing 0.5 mg of the corroded with 250 mg of KBr in an agate mortar after 2 hour vacuum drying, prior to forming a 12 mm diameter KBr disk by pressing.

Results

Mineral Precipitates in the Single PRB

The principal corrosion products of reactive ZVI medium are intermediate products (green rusts of GR I and GR II), hydrated forms of ferric oxides such as akaganeite (β-FeOOH), or lepidocrocite (ϒ-FeOOH), magnetite/maghemite, ferrihydrite, (phospho)siderite, and amorphous Fe phases (Fig. 2). The occurrence and relative contents of iron phases were slightly different according to column set-up with the electrode arrangement and the ZVI installation, the location of ZVI portion, which was either forward or backward from the influent entrance (Table 2). Because dissolved oxygen could be rapidly consumed at the entrance to the column by reacting with ZVI (Vogel and McCarthy, 1985), resulting in the generation of strong reducing condition behind portion of ZVI, the mineral assemblage of corrosive precipitates showed difference. A suite of minerals identified by the XRD patterns, which were formed in situ within the forward portion of ZVI barrier, were mainly akaganeite, lepidocrocite, magnetite/maghemite, (phospho)siderite, and ferrihydrite as well as the backward portion commonly included akaganeite, magnetite/maghemite, and green rusts (GRs). Amorphous Fe phases occurred in irregular distribution, and mackinaweite and iron sulfide were not found in this system.

Iron Oxyhydroxide (FeOOH) Precipitates

Akaganeite was the dominant phase because it transformed from $Fe(OH)_x^{3-x}$ with the nucleation of chloride ions (Schwertmann and Cornell, 2000) which was introduced by the dechlorination of TCE. Lepidocrocite was identified at the forward portion of ZVI, as mentioned above, due to the oxidation of GRs. Compared to that of unpacked fresh peerless Fe^0 filings (left), the corrosion surface of *Bc* column (right) filled with iron oxyhydroxides (akaganeite and lepidocrocite) had a GR mineral morphology, pseudo-hexagonal form (Fig. 3). Magnetite/maghemite was detected in every sample in our experiments.

Green Rusts

The GRs (GR I and GR II) showed two types of distribution in the column. One is only detected in the backward portion of ZVI, and the other is found in both of forward and backward portion (Fig. 2). This means that the consumption of DO at the forward portion made reducing condition at the backward. The gradual oxidation of GRs at pH 7.5 took over about 4 hours to lepidocrocite and some goethite in air (Schwertmann and Cornell, 2000; Phillips *et al.*, 2003). This indicates that the GRs occurring at the forward portion could readily transformed to lepidocrocite due to DO and pH increase. The XRD analyses could not confirm the type of GRs due to the trace amounts of this mineral. However, GR I (chloride and carbonate form), which had 7.5 Å peak and GR II (sulfate

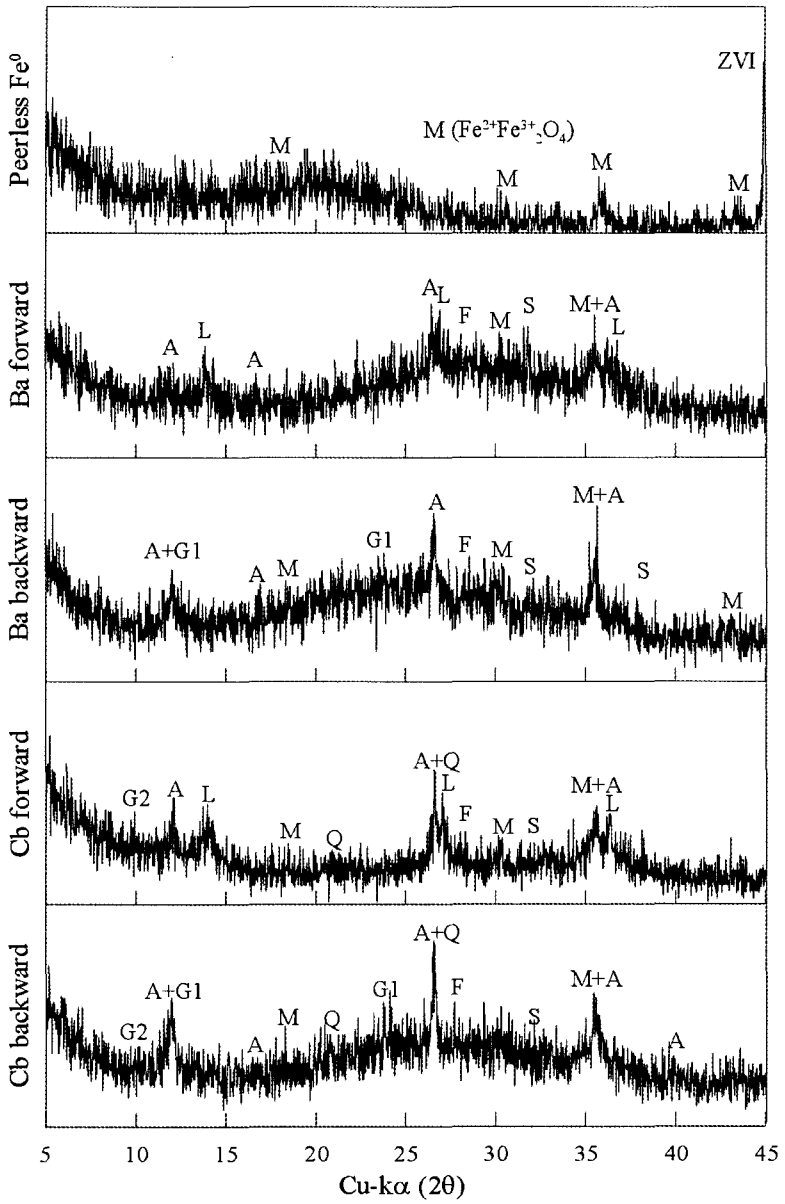

Fig. 2. Representative X-ray diffraction patterns. Front, back, and numbers mean the sampling site from the ZVI portion illustrate in Fig. 1. Abbreviations: A; akaganeite, F; ferrihydrite, G; goethite, G1; green rust I, G2; green rust II, L; lepidocrocite, M; magnetite/maghemite, S; (phospho)siderite, Q; quartz. Broad mound between 20~40° (2θ) indicates amorphous phases.

form), which had 9.0 Å peak were separately identified in the *Bb*-forward and *Cb*-backward samples (Génin *et al.*, 1998). SEM images showed some difference in shape. Forward portion had more irregular shaped Fe amorphous phases (Fig. 4a) and ferrihydrite (Fig. 4b). On the other hand, backward portion had more hexagonal shaped GRs (Fig 4e and f).

Table 2. Relative contents of mineral composition resulting from the TCE dechlorination

Sample	A	F	G	G1	G2	L	M	S	Q
Ba-forward	***	*				**	***	*	
Ba-backward	***	*		**			***	**	
Bb-forward	***	*		**	*	*	***	*	
Bb-backward	***			***			***		*
Bc	***	*			*	*	***	*	
Ca	***			*		**	***	*	**
Cb-forward	***	*			*		***		**
Cb-backward	***	*		**	*		***	*	**
Cc-forward	***	*					***	*	**
Cc-backward	***	*					***	*	**
Da-2	**					*	**	*	
Da-3	***			*			***	*	
Db-2	***	*		*		**	***	*	
Db-3	***					*	***		
Db-6	**						***		
Dc-2	***		*	**		**	***	*	
Dc-3	***			**		*	***	*	

Symbols: ***, major; **, minor; *, trace component.
Abbreviations: A; akaganeite, F; ferrihydrite, G; goethite, G1; green rust I, G2; green rust II, L; lepidocrocite, M; magnetite/maghemite, S; (phospho)siderite, Q; quartz.

Iron Carbonate/phosphate Precipitates

Gui and Devin (1994) found that the passivated iron film consisted of a mixture of ferrous and ferric oxyhydroxides and that their composition depended on the specific anions present in the solution. Because no other di- or tri-valent cations were added in the influent solution, (phospho)siderite [$Fe(PO_4 \cdot 2H_2O),(CO_3)$] was found to be the dominant carbonate/phosphate precipitate in the forward portion where groundwater enters the barrier.

Several factors such as pH, levels of carbonate, and Ca concentration may contribute to the above observation. Relatively high pH and high bicarbonate in combination with anaerobic environment, but low calcium concentrations favor the formation of siderite. Similarly siderite precipitation has been observed by Mackenzie *et al.* (1999). On the other hand, in this study, iron dissolved from ZVI and phosphate ions that have the highest electronegativity among used anions complexed and precipitated as (phospho) siderite.

Mineral Precipitates in the Double PRB

According to SEM examinations, the samples of portions 2 and 3, which were defined by the location of the ZVI portion (Fig. 1), showed predominantly uniform corrosion and were similar to forward and backward portion of ZVI in the single PRB. However, 6 portion sample looked like unreacted ZVI (Fig. 5).

The (phospho)siderites of portion 2 of *Dc* column occurred as an aggregate, which appeared similar to spherical shaped framboids (Fig. 6a). On the contrary, the distribution and occurrence of these aggregates at portion 3 was lower than those at portion 2 (Fig. 6i). The platy, hexagonal shaped GR had been transforming to FeO(OH) or magnetite/maghemite only having GR habit (Fig. 6b), because lepidocrocite and magnetite/maghemite were identified with GR by the XRD patterns. Ferrihydrite was also identified at front ZVI portion. However it

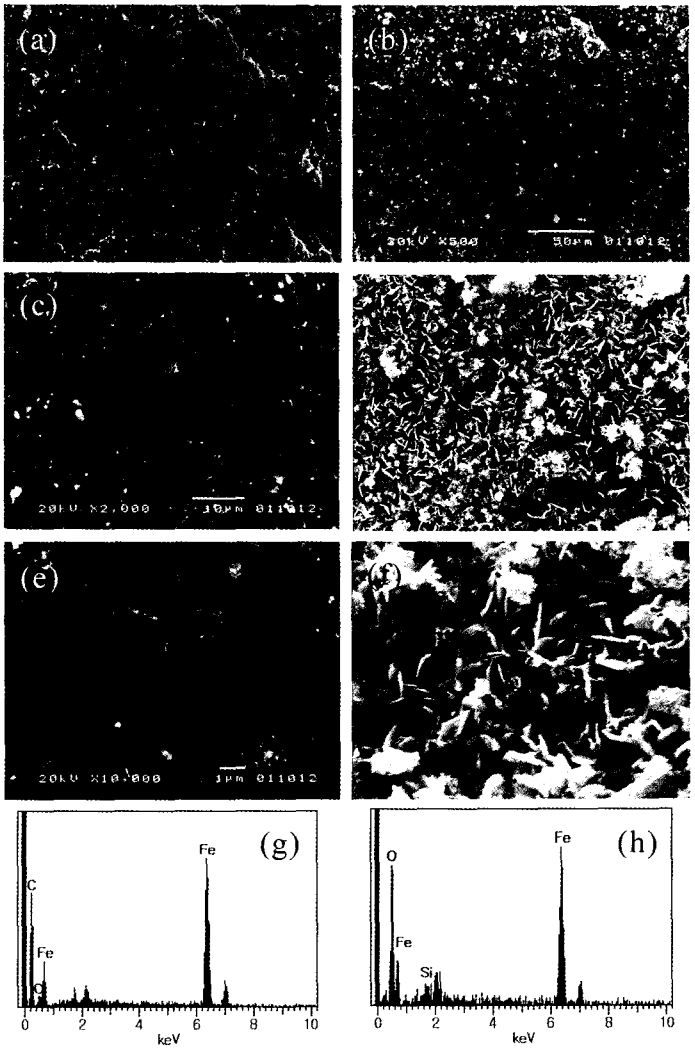

Fig. 3. Scanning electron microscopic images and EDX patterns of a representative corrosion surface of *Bc* column (b), (d), (f,) and (h) in comparison with unpacked peerless Fe^0 filings (a), (c), (e), and (g). Magnification was increased at the same site from (a) and (b) to (e) and (f).

showed delicate structure under the SEM observation at portion 2 (Fig. 6e) while lath-shaped ferrihydrite occurred at portion 3 (Fig. 6j). The (phospho)siderite is classified to monoclinic, so the rounded morphology of (phospho) siderite comes from the underlying mineral, particularly the rounded clusters of siderite crystals. This can be induced from the fact that HCO_3^- ions were also removed, but carbonate minerals were not detected. Therefore, with the initial, nucleated and precipitated siderite was subsequently coated and cemented by the phosphate ions. EDX patterns of spherical surface of (phospho) siderite just showed elemental P (Fig. 6i).

GR in backward portion of some columns had relatively low chloride content and the area of GR I was larger than that of GR II. Considering carbon coating for SEM observation, we cannot believe accuracy of carbon content, but amount of removed HCO_3^- ions might be used in production of the seed of (phospho)siderite, which occurred as a dominant cement material. Also, phosphate ions might be removed to form cement materials, (phospho)siderite, and amorphous Fe phosphate phases.

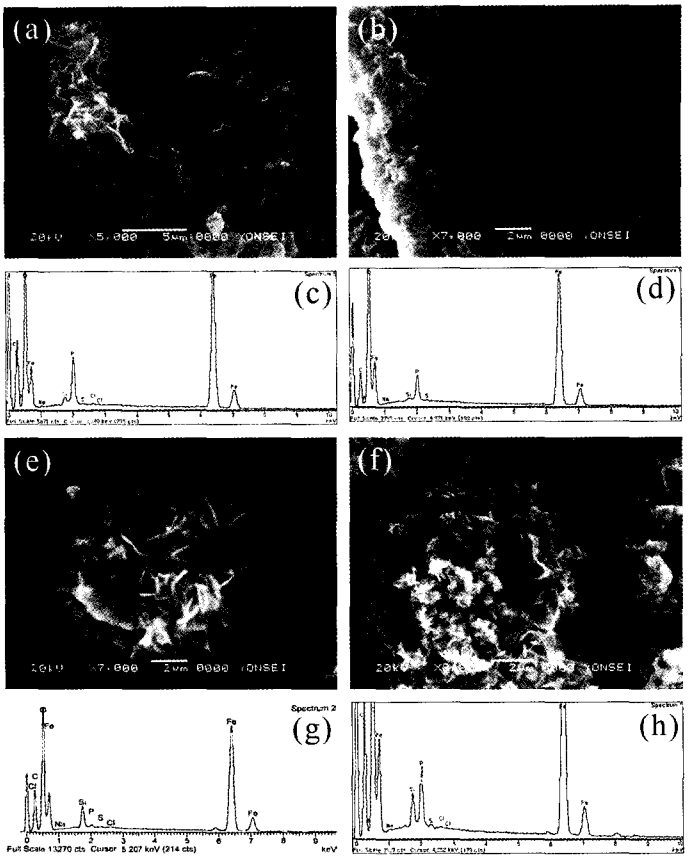

Fig. 4. Scanning electron microscopic images and EDX patterns of a representative corrosion surface of *Cb* column. (a) amorphous Fe phase, and (b) ferrihydrite in forward portion, (e) platy, hexagonal GR shaped FeO(OH), and (f) GR in backward portion, (c), (d), (g), and (h) EDX patterns of upper images.

Infrared Spectroscopic Characteristics of Corrosion Materials

In Fig. 7, infrared spectra showed distinct bands from the mixture of corrosion materials. Basically, absorption bands appearing at 3400 and 1630 cm^{-1} were caused by OH-stretching and H-O-H deformation due to adsorbed molecular water. Because pellets were pressed right after 2 hours vacuumed drying, consequently the bands could be normally identified as hydroxides and water molecules of iron (oxy)hydroxide, GR, etc. However, uniform, broad, band at 3427~3367 cm^{-1} could indicate ferrihydrite (Russell and Fraser, 1994).

In the range of 800~400 cm^{-1}, absorption bands indicate the bond between oxygen and other cations such as Si, Fe, Al, etc. (Van der Marcel and Beutelspacher, 1976). Small and sharp bands at 799 and 779 cm^{-1} were found to be quartz and overlapping Si-O bond on Fe-O bond caused strong band at around 470 cm^{-1}.

A small band (1082 cm^{-1}) may be attributed to magnetite (Van der Marcel and Beutelspacher, 1976), although typical bands of maghemite were detected at 1170, 691, and 636 cm^{-1}. Other band (1021 cm^{-1}) is attributed to lepidocrocite. Broad band at 1385~1362 cm^{-1} were maybe attributed to carbonates (Roh *et al.*, 2000b), which were detected as (phospho)siderite by XRD.

Like samples showing similar XRD patterns, semi-quantitative result through IR analysis indicated that more lepidocrocite and ferrihydrite or Fe (oxy)hydroxide formed in the forward samples, while backward samples have more magnetite/maghemite.

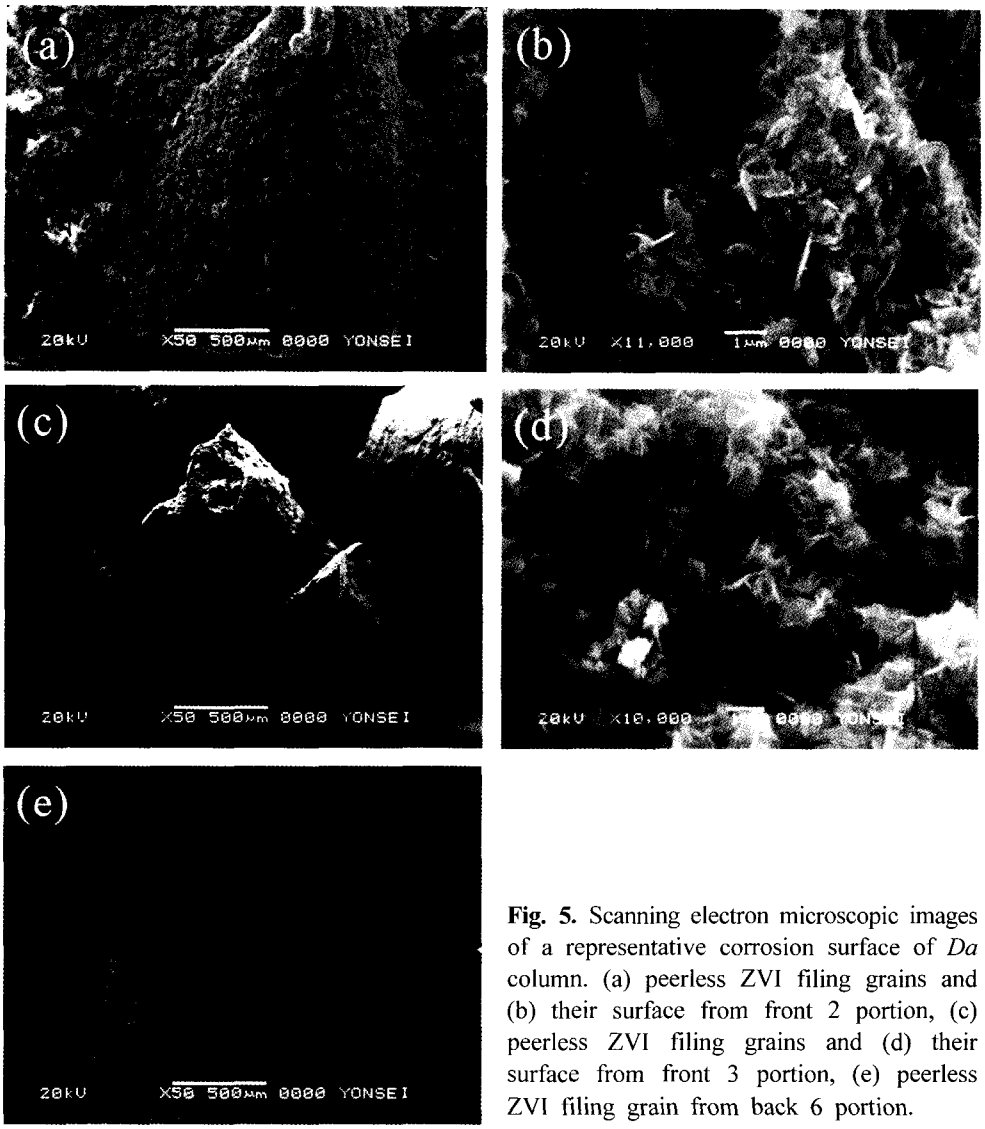

Fig. 5. Scanning electron microscopic images of a representative corrosion surface of *Da* column. (a) peerless ZVI filing grains and (b) their surface from front 2 portion, (c) peerless ZVI filing grains and (d) their surface from front 3 portion, (e) peerless ZVI filing grain from back 6 portion.

Anionic Characteristics of Effluents

While background solution passed through the columns, the relative concentration levels of nitrate and sulfate remained unvaried except small increase at the initial stage and that of chloride decreased to the termination of dechlorination of TCE. On the other hand, bicarbonate level showed severe variation, and phosphate remained the lowest level among five major anions (Fig. 8).

For a background solution, sodium salts of chloride, nitrate, phosphate, sulfate, and bicarbonate were used as an equivalent amount (0.1 or 0.2 mM). Based on the anion analysis, phosphate removal was dominant, and bicarbonate was the next. The increase of chloride was due to dechlorination of TCE and intermediate by-products such as dichloroethylene (DCE) isomers and vinyl chloride (VC), and that of sulfate and nitrate might be due to the break of MES buffer.

The trends of nitrate and sulfate ions which were mentioned above might reflect the pH

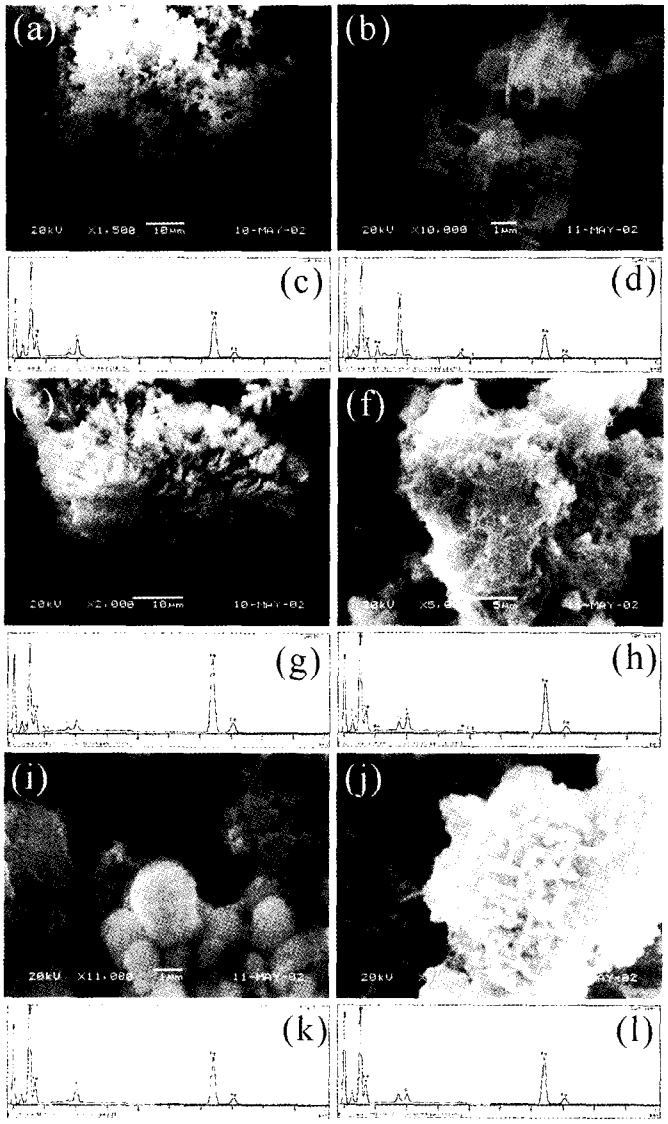

Fig. 6. Scanning electron images and EDX patterns of a representative corrosion surface of *Dc* column. (a) aggregates of (phospho)siderite, (b) transformed FeO(OH) from GR, (e) fine structured ferrihydrite, and (f) amorphous Fe phase from front 2 portion, (i) rarely occurred (phospho)siderite from front 3 portion than front 2, and (j) lath-shaped ferrihydrite from front 3 portion. (c), (d), (g), (h), (k), and (l) EDX patterns of upper images.

variations during the column experiment owing to the by-products, nitrate and sulfate, of MES buffer, although we can't estimate the anionic competition of these anions for precipitation under the different column set-up of E2PRB.

Discussion

Corrosion By-products During TCE Dechlorination

Mainly lepidocrocite, ferrihydrite, and (phospho) siderite identified by the XRD pattern, SEM images, and IR patterns were formed within the forward part of ZVI barrier, and magnetite/ maghemite and green rusts distinctively were in the backward part. Slightly more akaganeite was produced in backward part. The poorly crystalline akaganeite, which is, in general, easily formed and stable under the reduced groundwater conditions of the Fe^0 barrier for TCE remediation site (Phillips *et al.*, 2000; Roh *et al.*, 2000a), occurred with goethite (α-FeOOH). However, goethite occurred at only one sample during the column experiments. This means that

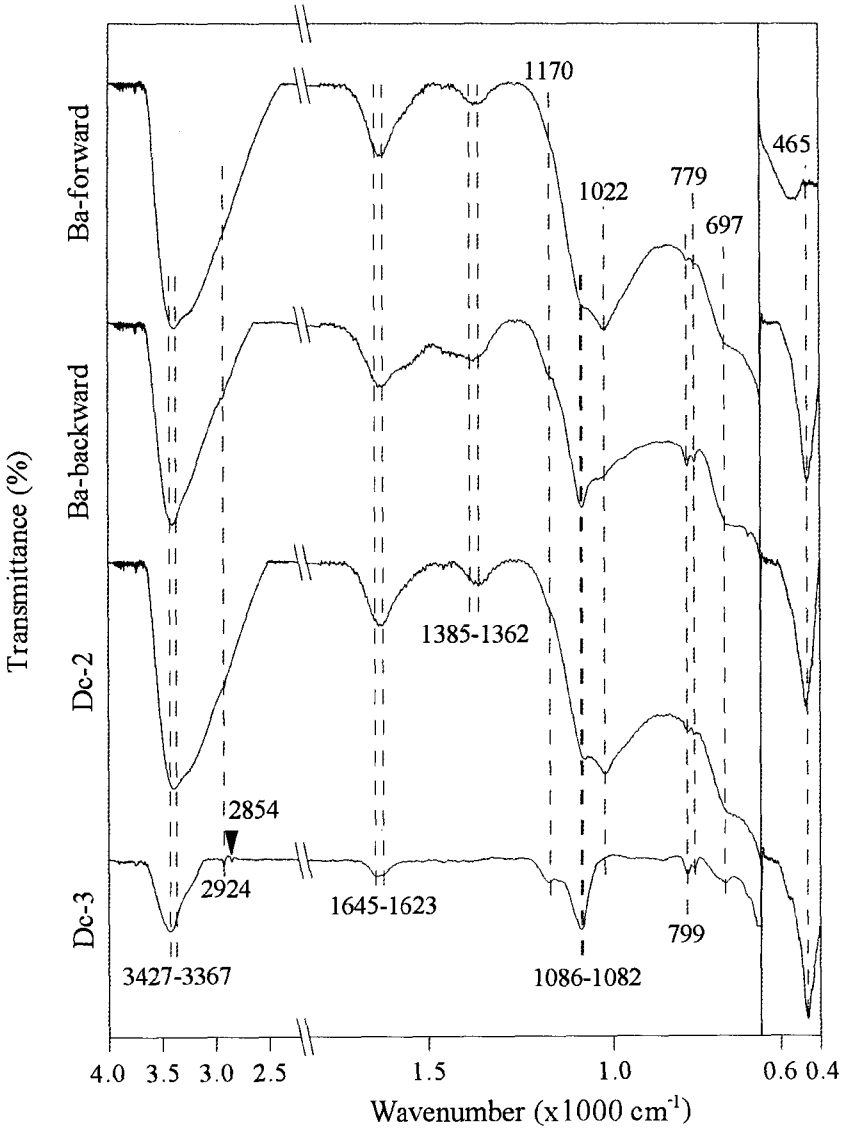

Fig. 7. Infrared spectra for corrosion materials of representative columns. Forward, backward, and numbers mean the sampling site from the ZVI portion illustrate in Fig. 1.

akaganeite was preferably formed by the nucleation of chloride ions (Schwertmann and Cornell, 2000) that were sufficiently supplied by the TCE dechlorination. Therefore, rare goethite distribution might be caused by the reductive environment, the short-term monitoring, and the anionic competition.

On the contrary, formation of lepidocrocite, which was favorable to forward portion, can be explained by the two facts of that GR occurred either at only backward portion or at both portions, and that the lepidocrocite is formed from the oxidation of GR (Schwertmann and Cornell, 2000). The influent containing DO consumed it at forward portion, so reducing condition in backward portion favord for the

formation of GRs. Therefore, GRs oxidized to lepidocrocite at forward portion, and could sustain at the backward portion. Sagoe-Crentsil and Glasser (1993) also showed similar result that GR was a stable corrosion product of pure iron at high pH and low Eh in the presence of chloride.

However, Srinivasan *et al.* (1996) found that the formation of lepidocrocite by a pathway involving GR II is an oversimplication of the actual process. During this process, small, dense, hexagonal Fe_3O_4 particles were formed in addition to, or instead of, the GR II hexagonal crystals. Abundant magnetite/maghemite co-existing with GR and lepidocrocite in the experiments, therefore, forward and backward portion might have lepidocrocite and more magnetite/maghemite, respectively, by oxidation of GR, although widely distributed platy hexagonal shaped by-product looked like GR.

In this study, the most widely occurring corrosion by-products, Fe oxyhydroxides, formed as a result of the corrosion of ZVI filings in groundwater with a concurrent release of Fe^{2+} and increased pH (Schwertmann and Taylor, 1989). The presence of Fe^{3+} and mixed Fe^{3+} and Fe^{2+} is due to DO in the groundwater (Watson *et al.*, 1999), and more oxidation from ferrous to ferric ion for TCE dechlorination, resulted in formation of GR I, GR II, Fe oxyhydroxides (akaganeite, lepidocrocite > goethite), and magnetite/maghemite. Precipitates composed of ferrous ion was just (phospho)siderite, which occurred at the forward portion.

Controlling Factors of Precipitation and Cementation

Many factors such as pH, the nature and the concentrations of anions, temperature, drying conditions, etc., may play significant roles in the evolution of the shape and structure of the final product (Srinivasan *et al.*, 1996). Controlling factors of precipitation and cementation was found to be pH, dissolved oxygen, the type of intermediate, anionic species to form complex strongly in this study. The pH condition was examined by abundant Fe oxyhydroxide and increased pH in the effluent Therefore, pH factors will be discussed here briefly.

pH

Another possibility of pH increase might be attributed to simulated groundwater, which had low ionic strength and buffering capacity (averaged EC value of 14 sources: 117 μS/cm) like a natural groundwater in equilibrium. Since used reagents having 0.1 ~ 0.2 mM concentration levels in simulated groundwater showed alkali in pH value ($NaHCO_3$, pH 8.86; $NaNO_3$, 8.45; Na_2SO_4, 8.39; NaCl, 8.38 in its concentration level), we controlled pH by adding acidic 2-(N-morpholino)ethanesulfonic acid (MES, molecular biology grade) as the biological buffer. However, the loss of buffer function of MES, as dechlorination with/without external DC processed, might cause pH increase with the hydrolysis at the cathode.

In Fig. 8, nitrate concentration in the effluent was high in *Ba*, *Bb* and *Cb* columns, and sulfate concentration was high in *Bb*, *Ca*, and *Cb* columns. These nitrate and sulfate anions, which were detected above the unit level of relative concentration (=1), might be derived from the break of MES buffer, therefore, it indicates that these columns had undergone rapid pH increase. Subsequently, high pH hindered the dissolution of ZVI and these columns showed relatively low removal efficiency (Moon *et al.*, in press).

The Type of Intermediates and Dissolved Oxygen

In precipitation reactions forming inorganic salts, the type of precursor may influence the structure and properties of the end products and one or more solute complexes may be involved (Srinivasan *et al.*, 1996).

Corrosion materials were mostly iron oxyhydroxide, magnetite/maghemite > GRs, ferrihydrite, (phospho)siderite, and lesser amount of

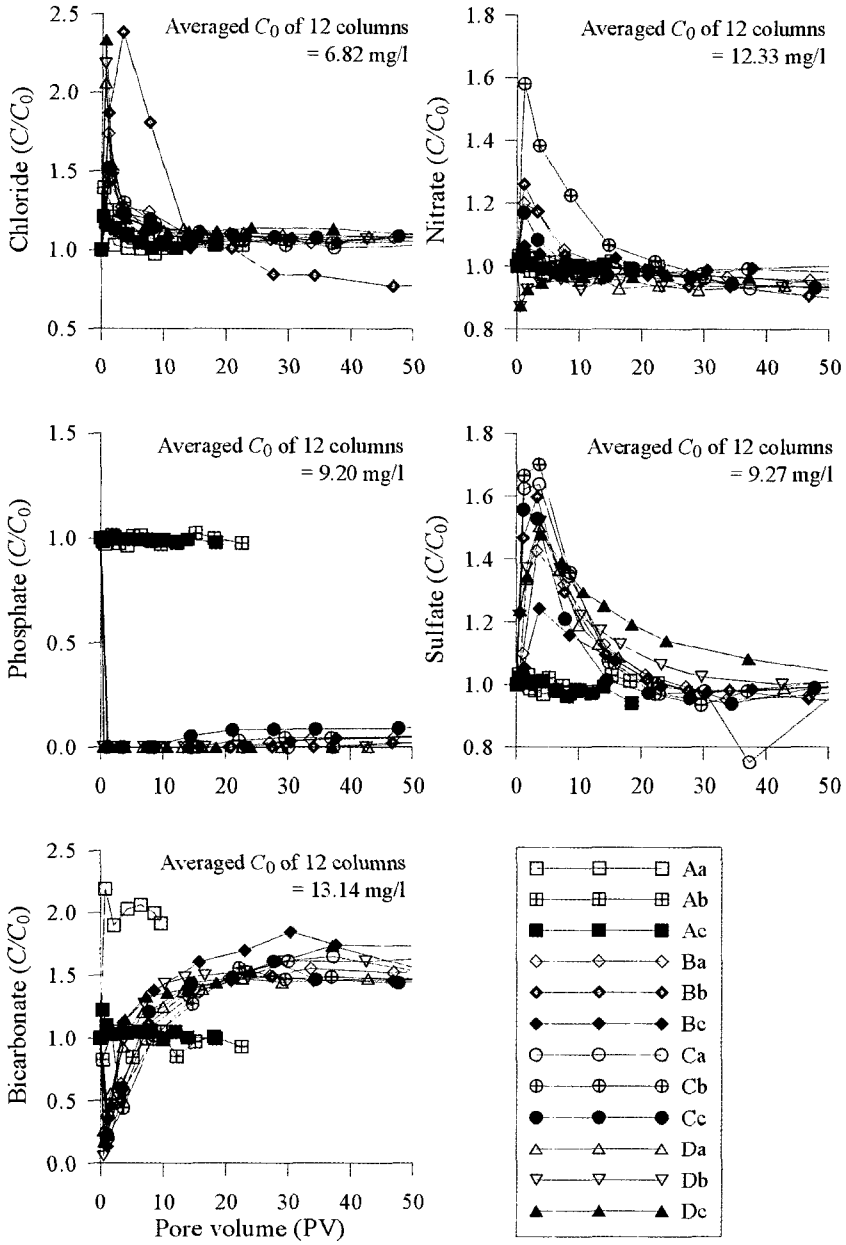

Fig. 8. Variations of relative concentrations of anion species through columns packed with different ZVI installation and electrode arrangement. C/C_0, the relative anion concentration; C and C_0, each anion concentration in the column effluent and influent, respectively.

amorphous Fe phases. Mackenzie *et al.* (1999) found that plugging occurred with water with no carbonate and high DO and did not occur with water with high carbonate and low DO. It could by varified by the fact that (phospho)siderite occurred at the forward portion rather than backward, because the forward portion was supplied with influent from the artificial ground-

water source including DO like the initial.

Anion species

HCO_3^- and SO_4^{2-}, which commonly occur in groundwater (Odziemkowskie *et al.*, 1998), are corrosive to ZVI (Gu *et al.*, 1999), and are expected to cause ZVI filings to disintegrate in reactive barriers. The accumulation of some precipitates, either individually or as a mixture, such as iron and calcium carbonate (Shoemaker *et al.*, 1995; Liang *et al.*, 1997), green rust (Edwards *et al.*, 1996), and iron oxyhydroxides may restrict flow and eventually clog the system (Mackenzie *et al.*, 1999, Shoemaker *et al.*, 1995).

The lowest relative concentration levels of phosphate mean that complexation with dissolved iron was the strongest even though we applied DC to the system (Fig. 8). In fact, carbonate shows stronger complexation (Langmuir, 1997), so that the reason of wide variation can be; one is analytical error due to air-exposure during the titration, and the other is bicarbonate, we supplied, transformed to carbonate by production of OH^- due to iron corrosion and electrolysis. This induction was supported by that the dominant carbonate mineral was (phospho)siderite, and that the nucleation of siderite consumed the transformed carbonate, then, siderite grew and was covered with (phospho)siderite.

The chemical formula of the carbonate GR I is $[Fe^{2+}{}_4Fe^{3+}{}_2(OH)_{12}][CO_3 \cdot 2H_2O]$ (Drissi *et al.*, 1995). In the absence of DO, Odziemkowski *et al.* (1998) found that the formation of carbonate GR I is thermodynamically unfavorable. In this study, occurrence of GR I was more dominant than GR II, this can be also explained by the competition among anions. However, we could not characterize if the GR I is either chloride or carbonate form due to carbon coating and poor peak separation on the EDX pattern by close position. The strong complexation of carbonate and low C/C_0 with the initial of bicarbonate might be consumed for the nucleation of (phospho)siderite.

On the contrary, slight increase of chloride content was due to dechlorination of TCE and those of nitrate and sulfate were owing to the breakdown of MES buffer. To date, there is no direct evidence showing an abiotic reduction of SO_4^{2-} by ZVI. The SO_4^{2-} green rust is also referred as GR II with a chemical formulation of $[4Fe(OH)_2 \cdot 2FeOOH \cdot FeSO_4 \cdot 4H_2O]$ (Refait and Génin, 1994). A continuous input of influent solution containing a low but nonzero concentration of DO would be expected to result in oxidation of some ferrous ions to ferric species even though the influent solutions were initially purged with N_2. Gui and Devine (1994) showed that in mildly acidic SO_4^{2-} solutions, SO_4^{2-} ions were not only adsorbed on to the surface of the passivated iron film but also covalently bonded and thus incorporated in the passivated film (presumably as GR II minerals). Although, GR II was detected by the XRD patterns (Fig. 2), the delay in formation of FeS was perhaps due to the greater length of time needed for an accumulation of a microbial population to facilitate SO_4^{2-} reduction.

Conclusion

The changes in degradation processes with time are attributed to (1) reduction in Fe surface reactivity caused by passivation of Fe^0 by precipitates, including Fe (hydr)oxides and other Fe phases as intermediate and end products of corrosion and Fe carbonate and phosphate as cementing and binding materials, and (2) alternation of flow paths through Fe filings as a result of precipitation and cementation.

Based on mineralogical study including XRD, SEM-EDX, FT-IR analysis, forward samples in the ZVI-based E2PRB, which had single ZVI portion, have more lepidocrocite, ferrihydrite or amorphous Fe phase, and (phospho)siderite while backward samples have more magnetite/maghemite and intermediate GR I and GR II. A suite of mineral distribution was related to the dissolved oxygen and increased pH. Double

E2PRB systems, which had two ZVI portions, produced similar corrosion products with a single E2PRB at 2 and 3 samples in the front ZVI.

Conclusively, removal efficiency considering precipitation, which implies loss of remediation capacity, was found to be more related to the electrode arrangement, basically cathodic protection. Controlling factors of E2PRB system were found to be (1) pH, (2) dissolved oxygen, (3) the type of intermediate, and (4) anionic species to form complex strongly.

Therefore, close attention should be given to locations in barriers that seem more vulnerable to corrosion (i.e. where groundwater first enters barriers), precipitation and subsequent cementation of Fe^0 filings. Future problems with PRB systems can be predicted and avoided with information gathered from mineralogical and geochemical studies of preexisting PRB systems.

Acknowledgement

This research was supported by the Korea Science and Engineering Foundation (Grant no. R01-2000-000-00057-0).

References

Deutsch, W.J. (1997) Water/rock interactions. in: Groundwater geochemistry - Fundamentals and application to contamination. (eds) Lewis Publishers, Boca Raton, p. 47-75.

Drissi, S.H., Refait, P.H., Abdelmoula, M., and Génin, J.M.R. (1995) The preparation and thermodynamic properties of Fe(II)-Fe(III) hydroxide-carbonate (green rust I); Pourbaix diagram of iron in carbonate-containing aqueous media. Corros. Sci., 37, 2025-2041.

Edwards, R.W., Duster, D., Faile, M., Gallant, W., Gilbeau, E., Myller, B., Nevling, K., and O'Brady, B. (1996) Presented at RTDF permeable reactive barriers action team meeting, San Francisco, CA., August 15-16.

Génin, J.M.R., Bourrié, G., Trolard, F., Abdelmoula, M., Jaffrezic, A., Refait, P., Maitre, V., Humbert, B., and Herbillon, A. (1998) Thermodynamic equilibria in aqueous suspensions of synthetic and natural Fe(II)-Fe(III) green rusts: Occurrence of the mineral in hydromorphic soils. Environ. Sci. Technol., 32, 1058-1068.

Gu, B., Phelps, T.J., Liang, L., Dickey, M.J., Roh, Y., Kinsall, B.L., Palumbo, A.V., and Jacobs, G.K. (1999) Biogeochemical dynamics in zero-valent iron columns: Implication for permeable reactive barriers. Environ. Sci. Technol., 33, 2170-2177.

Gui, J. and Devine, T.M. (1994) The influence of sulfate ions on the surface enhanced Raman spectra of passive films formed on iron. Corros. Sci., 36, 441-462.

Gui, J. and Devine, T.M. (1995) A SERS investigation of the passive films formed on iron in mildly alkaline solutions of carbonate/bicarbonate and nitrate. Corros. Sci., 37, 1177-1189.

Langmuir, D. (1997) Aqueous complexes. in: Aqueous environmental geochemistry, (eds) Prentice Hall, New Jersey, p.82-122.

Liang, L., West, O.R., Korte, N.E., Goodlaxson, J.D., Pickering, D.A., Zutman, J.L., Anderson, F.J., Welch, C.A., Pelfrey, M.J., and Dickey, M.J. (1997) The X-625 groundwater treatment facility: A field-scale test of trichloroethylene dechlorination using iron filings for the X-120/X-749 groundwater plume. ORNL/TM-13410, Oak Ridge National Laboratory, Oak Ridge, TN, 63p.

Matheson, L.J. and Tratnyek, P.G. (1994) Reductive dehalogenation of chlorinated methanes by iron metal. Environ. Sci. Technol., 28, 2045-2053.

Mackenzie, P.D., Horney, D.P., and Sivavec, T.M. (1999) Mineral precipitation and porosity losses in granular iron columns. J. Hazard. Mater., 68, 1-17.

Moon, J.-W., Moon, H.-S., Roh, Y., Lee, S.Y., and Song, Y. (2001) Preliminary experiments for the remediation of trichloroethene-contaminated groundwater using direct current and zero-valent iron. Econ. Environ. Geol., 34, 307-313 (in Korean).

Moon, J.-W., Moon, H.-S., Roh, Y., Kim, H., and Song, Y. (2002) Optimal remediation of TCE-contaminated groundwater using direct current and Fe^0. Econ. Environ. Geol., 35, 229-239 (in Korean).

Moon, J.-W., Moon, H.-S., Roh, Y., Kim, H., and Lee, S.Y. (in press) Electro-enhanced permeable reactive barrier 1. Experimental results of op-

timal design for abiotic remediation of TCE contaminated groundwater according to zero valent iron installation and electrode arrangements. J. Contam. Hydrol.

Odziemkowski, M.S., Schuhmacher, T.T., Gillham, R.W., and Reardon, E.J. (1998) Mechanism of oxide film formation on iron in simulating groundwater solutions: Raman spectroscopic studies. Corros. Sci., 40, 371-389.

Page, M.M. and Page, C.L. (2002) Electroremediation of contaminated soils. J. Environ. Eng., 128, 208-219.

Phelps, T.J., Niedzielski, J.J., Malachowsky, K.J., Schram, R.M., Herbes, S.E., and White, D.C. (1991) Biodegradation of mixed-organic wastes by microbial consortia in continuous-recycle expanded-bed bioreactors. Environ. Sci. Technol., 25, 1461-1465.

Phillips, D.H., Gu, B., Watson, D.N., and Roh, Y. (2003) Impact of sample preparation on mineralogical analysis of Fe(0) reactive barrier materials. J. Environ. Qual., 32 (In Press).

Phillips, D.H., Gu, B., Watson, D.N., Roh, Y., Liang, L., and Lee, S.Y. (2000) Performance evaluation of a zero-valent iron reactive barrier: Mineralogical characteristics. Environ. Sci. Technol., 34, 4169-4176.

Reardon, E.J. (1995) Anaerobic corrosion of granular iron: Measurement and interpretation of hydrogen evolution rate. Environ. Sci. Technol., 29, 2936-2945.

Refait, P.H. and Génin, J.M.R. (1994) The transformation of chloride-containing green rust I into sulphated green rust II by oxidation in mixed Cl^- and SO_4^{2-} aqueous media. Corros. Sci., 36, 55-65.

Roh, Y., Lee, S.Y., and Elless, M.P. (2000a) Characterization of corrosion products in the permeable reactive barriers. Environ. Geol., 40, 184-194.

Roh, Y., Lee, S.Y. Elless, M.P., and Foss, J.E. (2000b) Incorporation of radioactive contaminants into pyroaurite-like phases by electrochemical synthesis. Clays Clay Miner., 48, 266-271.

Roh, Y., Lee, S.Y., Elless, M.P., and Moon, H.-S. (2000c) Electro-enhanced remediation of trichloroethene-contaminated groundwater using zero-valent iron. Environ. Sci. Health, Part A, 35, 1061-1076.

Russell, J.D. and Fraser, A.R. (1994) Infrared methods. in: Clay mineralogy: Spectroscopic and chemical determinative methods, (eds) Wilson, M.J., Chapman & Hall, London, p.11-67.

Sagoe-Crentsil, K.K. and Glasser, F.P. (1993) Constitution of green rust and its significance to the corrosion of steel in Portland cement. Corrosion, 49, 457-463.

Schwertmann, U. and Cornell, R.M. (2000) Iron oxides in the laboratory: Preparation and characterization, 2nd (eds), Wiley-VCH Publishers, New York. 188p.

Schwertmann, U. and Taylor, R.M. (1989) Iron oxides. in: Minerals in soil environments, (eds) Dixon, J.B. and Weed, S.B., SSSA Book series, no.1, Soil Science Society of America, Madison, WI, p.379-438.

Shoemaker, S.H., Greiner, J.F., and Gillham, R.W. (1995) In Assessment of barrier contaminant technologies. (eds) Rumer, R.R. and Mitchell, J.K., U.S. Department of Energy, Washington, D.C., p. 301-353.

Srinivasan, R., Lin, R., Spicer, R.L., and Davis, B.H. (1996) Structural features in the formation of the green rust intermediate and ϒ-FeOOH. Colloid. Surface. A, 113, 97-105.

Tratnyek, P.G., Johnson, T.L., Scherer, M.M., and Eykholt, G.R. (1997) Remediating ground water with zero-valent metals: Chemical considerations in barrier design. Ground Water Monit. Remed., 17, 108-114.

Van der Marcel, H.W. and Beutelspacher, H. (1976) Atlas of infrared spectroscopy of clay minerals and their admixtures. (eds) Elsevier Scientific Publishing Company, Amsterdam, 396p.

Vogel, T.M. and McCarty, P.L. (1985) Biotransformation of tetrachloroethylene to trichloroethylene, dichloroethylene, vinyl-chloride, and carbon-dioxide under methanogenic conditions. Appl. Environ. Microb., 49, 1080-1083.

Watson, D., Gu, B., Phillips, D.H., and Lee, S.Y. (1999) Evaluation of permeable reactive barriers for removal of uranium and other inorganics at the Department of Energy Y-12 Plant, S-3 disposal ponds; ORNL/TM-1999-143; Oak Ridge National Laboratory; Oak Ridge, TN.

2003년 2월 27일 원고접수, 2003년 3월 15일 게재승인.